X International Conference on Computational Methods in Marine Engineering
MARINE 2023
J. García-Espinosa, L. González, J.E. Gutiérrez & B. Serván-Camas (Eds)

Transfer Function Estimation with a Numerical Harmonic Probing Algorithm

David Stamenov[*], Giuseppe Abbiati[†] and Thomas Sauder[††]

[*†] Department of Civil and Architectural Engineering, Aarhus University, Inge Lehmanns Gade 10, Aarhus, Denmark

[††] SINTEF Ocean, P.O. Box 4762 Torgarden, 7465 Trondheim, Norway

[††] Department of Marine Technology, Norwegian University of Science and Technology, Trondheim 7491, Norway

ABSTRACT

Moored systems exhibit low stiffness in the horizontal degrees of freedom. This results in the structure having low natural frequencies and being sensitive to the low-frequency second order loads. Low-frequency loads arise as a result of inter-modulation of the wave frequencies. Accurate modeling of the low-frequency hydrodynamic loads is of crucial importance for developing cost-competitive floater designs. This study implements a Kriging-NARX model for forecasting hydrodynamic loads and a harmonic probing algorithm for extracting the transfer functions of the system. The implemented harmonic probing method is of numerical nature and avoids the use of computationally expensive symbolic coding tools. The method was tested on the INO WINDMOOR 12 MW floater for extracting the structure's linear transfer function. The obtained transfer function results showed an excellent agreement with potential flow and symbolic harmonic probing.

Keywords: NARX; Harmonic Probing; Transfer Function; Autoregressive; Hydrodynamic Loading.

NOMENCLATURE

f_n	Model output for time-step n [N]
F_n	Frequency domain representation of the response [-]
$\mathcal{F}$	Nonlinear autoregressive model [-]
$h^{(n)}$	n^{th} order impulse response function [N m^{-1}]
$H^{(n)}$	n^{th} order transfer function [N m^{-1}]
H_s	Significant wave height [m]
k	Squared exponential correlation function [-]
$\mathbf{r}$	Residual signal in time domain [-]
$\mathbf{R}$	Residual signal in frequency domain [-]
S	JONSWAP spectrum [m^2 s]
$\mathbf{t}$	Time vector [s]
T_p	Wave period [s]
$\mathbf{x_n}$	Combined input vector, autoregressive and exogenous part [N, ..., N, m, ..., m]
Z_n	Frequency domain representation of the input [-]
ϵ	Random number between 0 and 2π [-]
ζ_n	Model input for time-step n [m]
θ_f	Scale length of the autoregressive input [-]
θ_ζ	Scale length of the exogenous input [-]
σ_e	Noise variance [-]
σ_f	Optimization hyperparameter [-]
ϕ	Phase angle [rad]
Ω, ω	Angular frequency [rad/sec]
LTF	Linear Transfer Function
QTF	Quadratic Transfer Function
NARX	Nonlinear Autoregressive Model with Exogenous Input

1. INTRODUCTION

1.1 Background and Motivation

Linear models, to a large extent, can successfully describe the wave-induced motions and loads on large-volume structures in mild sea states where viscous effects are negligible (Faltinsen, 1990). However, one limiting factor of linear models is that inter-modulation is not possible i.e. no energy can be transferred between frequencies. This means that the computed steady-state output of a linear system to a regular wave will only match the frequency of the wave. Yet, in situ measurements and model scale experiments show that loads and responses do not occur only at the wave frequencies (Molin, 2023). An incoming bi-chromatic wave with frequencies f_1 and f_2 excites the individual frequencies separately but also any combination of sum $|f_1 + f_2|$, difference $|f_1 - f_2|$, or multiples $(2f_1, 3f_1, \ldots, 2f_2, 3f_2, \ldots)$ of the wave frequencies. Most structures are insensitive to these higher-order loads which means a linear model is sufficient for their design. However, moored structures, for example, are characterized by low natural frequencies in the horizontal degrees of freedom due to their soft mooring systems. As a consequence, their natural frequencies fall in the range where the difference frequency loads operate. For that reason, a significant contribution to the tension in the mooring lines at the extreme offsets comes from the mean drift force and the low-frequency loads that are usually described by a difference quadratic transfer function (QTF). The QTF, together with the second order loading, is more difficult to compute accurately. Potential flow-based solvers have been the main tool for estimating these loads

though they are limited to an incompressible and irrotational flow of an inviscid fluid. Nevertheless, potential flow and perturbation theory have provided an excellent basis for offshore engineering in mild sea-states. Moderate-to-extreme sea states with steep waves violate these assumptions which leads to inaccuracies in the transfer function (TF) estimation. Sauder (2021) provides an excellent overview of the limitations of potential flow theory and the challenges related to computing hydrodynamic properties of floaters. The theoretical limitations of the engineering tools result in an added uncertainty which is usually manifested as a larger safety factor and essentially a structurally more inefficient design. For that reason, an accurate estimation of the hydrodynamic loads is crucial for providing cost-competitive floater designs.

This study focuses on an alternative, data-driven approach for estimating hydrodynamic loading on floating structures. More specifically, the focal point is an improvement of an already existing method for extracting higher order transfer functions. Namely, the harmonic probing (HP) method which is used in tandem with a nonlinear autoregressive models with exogenous input (NARX). A quick overview of both is provided in the next section.

1.2 Scope

The origin of NARX models dates back to the work of Billings in the 1980s when the ARMAX (auto-regressive moving average model with exogenous inputs) was extended to its nonlinear form i.e. the NARMAX model (Leontaritis and Billings, 1985a,b). This framework is the most generic and versatile formulation of a nonlinear discrete-time process that incorporates a noise model and is usually given a polynomial form. A simplification to the NARMAX model is the NARX model which assumes that the noise process is white Gaussian (Worden et al., 2012). When coupled with harmonic probing (HP), the NARX framework allows for an estimation of any order transfer function. The algorithm for harmonic probing was first introduced by Bedrosian and Rice (1971) for continuous-time systems where the underlying equations of motion are known. They presented two approaches for extracting higher-order frequency response functions, namely, the harmonic input method and the direct expansion method. Peyton-Jones and Billings (1989) modified the harmonic input method into a recursive algorithm for computing an arbitrary order transfer function. This method, also known as harmonic probing, was later extended to discrete-time systems by Tsang and Billings (1992). Worden and Tomlison (2001) and Billings (2013) provide a more extensive overview and worked out examples of this procedure. The harmonic probing method is based on constructing harmonic balances and equating coefficients that require symbolic evaluation. Consequently, for complex systems with many lags resulting in a large number of polynomial terms, the length of the balancing expression grows fast which renders the whole procedure intractable. To circumvent this issue, Bayma and Lang (2012) developed a numerical procedure based on the Diophantine equations that reduces the computation demand though its implementation requires more effort (Billings, 2013).

The present paper describes a variant of the harmonic probing algorithm that is based on the original implementation but evades the use of the costly symbolic evaluation. The algorithm is applied to a Kirging-NARX model for extracting the **linear** transfer function (LTF) of the INO WINDMOOR 12 MW floater. The algorithm is generic and can be used for estimating an arbitrary order of a system's transfer function.

The remaining of the paper is structured as follows. First, Section 2 provides the underlying theory of the NARX model used in this study which is based on the works of Worden and colleagues (Worden et al., 2012; Worden and Tomlison, 2001; Worden et al., 2018). Section 3 follows with a description of the basics of harmonic probing together with the symbolic and numerical probing algorithms. The

study finishes with a case study of a floater in Section 4 and concluding remarks in Section 5.

2. KRIGING-NARX

The main idea behind NARX (nonlinear auto-regressive model with exogenous input) is to construct and train a model ($\mathcal{F}$) such that it can provide a prediction of the current output based on past input and output data.

$$f_n = \mathcal{F}\left(\underbrace{f_{n-1}, f_{n-2}, \dots, f_{n-n_f}}_{\text{auto-regressive part } \mathbf{x}_{f,n}}; \underbrace{\zeta_n, \zeta_{n-1}, \zeta_{n-2}, \dots, \zeta_{n-n_\zeta}}_{\text{exogenous part } \mathbf{x}_{\zeta,n}}\right) \tag{1}$$

$$f_n = \mathcal{F}\left(\mathbf{x}_n\right) \tag{2}$$

where $f_n \in \mathbb{R}$ is the output of the model for the current time-step t_n. The lagged values $\mathbf{x}_{f,n} = \left[f_{n-1}, f_{n-2}, \dots, f_{n-n_f}\right]$ of the load and the lagged values $\mathbf{x}_{\zeta,n} = \left[\zeta_n, \zeta_{n-1}, \zeta_{n-2}, \dots, \zeta_{n-n_\zeta}\right]$ of the wave elevation profile are concatenated to form the input vector $\mathbf{x}_n = [\mathbf{x}_{f,n}, \mathbf{x}_{\zeta,n}] \in \mathbb{R}^{n_f+n_\zeta+1}$. The optimal selection of the time-step $\Delta t = t_n - t_{n-1}$ depends on the dynamics of the modeled system.

Kriging-NARX is a special type of NARX that employs the concept of Kriging. Kriging dates back to the 1950s when it was first introduced in geostatistics (Krige, 1951). Since then, the machine learning community has re-purposed Kriging for a variety of learning tasks. The book by Rasmussen and Williams (2006) provides a good overview of this methodology, a consolidated summary is presented hereafter.

The underlying assumption of Kirging-NARX is that the model output is a realization of a Gaussian process (GP) (Santner et al., 2019). From the definition of a GP it follows that the distribution for a finite number of outputs follows a multivariate joint normal distribution.

$$\begin{pmatrix}\begin{bmatrix} f_n \\ f_{n-1} \\ f_{n-2} \\ \vdots \end{bmatrix}\end{pmatrix} \sim \mathcal{N}\left(\begin{bmatrix} 0 \\ 0 \\ 0 \\ \vdots \end{bmatrix}, \begin{bmatrix} k(\mathbf{x}_n, \mathbf{x}_n) + \sigma_e^2 & k(\mathbf{x}_n, \mathbf{x}_{n-1}) & k(\mathbf{x}_n, \mathbf{x}_{n-2}) & \dots \\ k(\mathbf{x}_{n-1}, \mathbf{x}_n) & k(\mathbf{x}_{n-1}, \mathbf{x}_{n-1}) + \sigma_e^2 & k(\mathbf{x}_{n-1}, \mathbf{x}_{n-2}) & \dots \\ k(\mathbf{x}_{n-2}, \mathbf{x}_n) & k(\mathbf{x}_{n-2}, \mathbf{x}_{n-1}) & k(\mathbf{x}_{n-2}, \mathbf{x}_{n-2}) + \sigma_e^2 & \dots \\ \vdots & \vdots & \vdots & \ddots \end{bmatrix}\right) \tag{3}$$

Notice that the mean of the joint distribution is assumed to be zero for simplicity. The method allows for a non-zero mean joint distribution though this adds additional model complexity and training parameters. In the above expression, the hyperparameter σ_e^2 is the noise variance which in itself incorporates a nugget for numerical stability, whereas $k(\cdot, \cdot)$ is a correlation function selected by the user. A number of correlation functions and their applications are listed in (Lataniotis et al., 2022). A common choice is the squared exponential correlation function which is infinitely differentiable leading to smooth paths. This function was the natural choice for this study since the signals investigated here are of smooth nature. The squared exponential function was modified to include a scaling length on both input signals leading to the following expression:

$$k([\mathbf{x}_{f,p}, \mathbf{x}_{\zeta,p}], [\mathbf{x}_{f,q}, \mathbf{x}_{\zeta,q}]) = \sigma_f^2 \exp\left(-\frac{1}{2\theta_f^2}\|\mathbf{x}_{f,p} - \mathbf{x}_{f,q}\|^2 - \frac{1}{2\theta_\zeta^2}\|\mathbf{x}_{\zeta,p} - \mathbf{x}_{\zeta,q}\|^2\right) \tag{4}$$

where $\|\quad\|$ is the Euclidean norm of the given vector difference while $\mathbf{x}_f$ and $\mathbf{x}_\zeta$ refer to the auto-regressive and exogenous part of the input vector, respectively. The expression above introduces three new hyperparameters: σ_f and the scale lengths, θ_f and θ_ζ. Assume now that the training data is

gathered as follows:

$$\mathbf{F} = \begin{bmatrix} f_{n-1} \\ \vdots \\ f_{n-N} \end{bmatrix}, \mathbf{X} = \begin{bmatrix} f_{n-2} & \cdots & f_{n-n_f} & \zeta_{n-1} & \cdots & \zeta_{n-n_\zeta} \\ \vdots & \ddots & \vdots & \vdots & \ddots & \vdots \\ f_{n-N-1} & \cdots & f_{n-N-n_f} & \zeta_{n-N} & \cdots & \zeta_{n-N-n_\zeta} \end{bmatrix} \tag{5}$$

with N representing the total number of data points. Then, the expression from (3) can be represented in a matrix form:

$$\begin{pmatrix} f_n \\ \mathbf{F} \end{pmatrix} \sim \mathcal{N}\left(\mathbf{0}, \begin{bmatrix} K(\mathbf{x}_n, \mathbf{x}_n) + \sigma_e^2 & \mathbf{K}(\mathbf{X}, \mathbf{x}_n) \\ \mathbf{K}(\mathbf{x}_n, \mathbf{X}) & \mathbf{K}(\mathbf{X}, \mathbf{X}) + \sigma_e^2 \mathbf{I} \end{bmatrix} \right) \tag{6}$$

The advantage of the joint Gaussian distribution is that the distribution of the unknown output f_n for an unobserved input $\mathbf{x}_n$ pre-conditioned on a set of observation $\{\mathbf{X}, \mathbf{F}\}$ is also Gaussian. From (6), the corresponding mean and variance for the output f_n have analytical expressions, which read,

$$\mathbb{E}[f_n|\mathbf{F}, \mathbf{X}] = \mathcal{F}(\mathbf{x}_n) = \mathbf{K}(\mathbf{x}_n, \mathbf{X})[\mathbf{K}(\mathbf{X}, \mathbf{X}) + \sigma_e^2 \mathbf{I}]^{-1} \mathbf{F} \tag{7}$$

$$\mathbb{V}[f_n|\mathbf{X}] = K(\mathbf{x}_n, \mathbf{x}_n) - \mathbf{K}(\mathbf{x}_n, \mathbf{X})[\mathbf{K}(\mathbf{X}, \mathbf{X}) + \sigma_e^2 \mathbf{I}]^{-1} \mathbf{K}(\mathbf{X}, \mathbf{x}_n) + \sigma_e^2 \tag{8}$$

Notice above that the expectation is preconditioned on the past outputs $\mathbf{F}$ and also the training data $\mathbf{X}$. That is, the training data become a part of the model equations and permanently "lives" in the algorithm. This feature provides an advantage of Kriging-NARX because it reduces the number of hyperparameters needed to capture the relationship of the modeled signals. In addition, this means that the model can be successfully trained with a relatively small amount of data.

The only remaining part is to close Eq. (7), i.e. train the unknown hyperparameters, $\theta^* = [\sigma_f^2, \sigma_e^2, \theta_f, \theta_\zeta]$. Training is performed by using a maximum likelihood estimation over a marginal evidence function. Put simply, since the outputs (or observations) $\mathbf{F} = \{\mathcal{F}(\mathbf{x}_1), \mathcal{F}(\mathbf{x}_2), \ldots, \mathcal{F}(\mathbf{x}_N)\}$ are assumed to have a joint normal distributed, maximizing their likelihood means finding the zero-mean joint normal distribution that best fits the data. For a given set of training data, $(\mathbf{F}, \mathbf{X})$, the likelihood function takes the following form:

$$\mathcal{L}(\theta^*, \mathbf{F}, \mathbf{X}) = \frac{(\det\big(\mathbf{K}(\mathbf{X}, \mathbf{X}) + \sigma_e^2 \mathbf{I}\big))^{-1/2}}{(2\pi)^{N/2}} \exp\left(-\frac{1}{2} (\mathbf{F}^T [\mathbf{K}(\mathbf{X}, \mathbf{X}) + \sigma_e^2 \mathbf{I}]^{-1} \mathbf{F} \right) \tag{9}$$

In practice, the hyperparameter values are obtained by minimizing the negative log likelihood function, which reads,

$$\theta^* = \arg\min_{\theta^*}[\log(\mathcal{L})] = \arg\min_{\theta^*} \frac{1}{2} \mathbf{F}^T \left[\mathbf{K}(\mathbf{X}, \mathbf{X}) + \sigma_n^2 \mathbf{I}\right]^{-1} \mathbf{F} + \frac{1}{2} \log\big(\det\big(\mathbf{K}(\mathbf{X}, \mathbf{X}) + \sigma_e^2 \mathbf{I}\big)\big) \tag{10}$$

Note that the dependence on the optimization parameters θ^* is not explicitly shown above, but it is rather obvious from (4). Furthermore, the $\frac{N}{2}\log(2\pi)$ term is left out since it does not affect the optimization. Due to the low number of hyperparameters to be optimized, the training can be completed with a simple gradient descent optimization algorithm. Note also from (10) that the optimization requires a matrix inversion. The matrix $\mathbf{K}(\mathbf{X}, \mathbf{X})$ is of $N \times N$ size, where N is the number of observations in the training set. Since the numerical optimization algorithms rely on repeated evaluations of the objective function, the optimization may become costly for large data sets. Once the training is complete, the model Eq. (7) can be readily evaluated for a set of two new signals originating from the same underlying process for which the model was trained for. An application of this framework is presented in Section 4.

3. HARMONIC PROBING

The Kriging-NARX described in the previous section is one of many possible NARX models. Although useful for time series modeling, in general, engineers are interested in obtaining both LTF and QTF associated with a hydrodynamic loading model. The harmonic probing (HP) algorithm provides the connection between the mathematics-based NARX model and its Volterra series representation. Consequently, this allows for the extraction of the Generalized Frequency Response Functions (GFRF). A good overview of HP is available in Chapter 8 of (Worden and Tomlison, 2001). A condensed description is presented hereafter starting with the fundamental equations of a Volterra expansion and moving on to the symbolic and then the novel numerical probing.

3.1 Volterra Series Expansion

The Volterra series expansion is a convenient way to represent dynamic systems with weak nonlinearities and computing GFRFs (Billings, 2013). Weiner (1942) applied the Volterra series expansion to nonlinear systems and noted the existence of a functional relationship between the input and output of the system:

$$f(t) = f^{(0)} + f^{(1)}(t) + f^{(2)}(t) + \cdots + f^{(m)}(t) \tag{11}$$

where f^0 is a constant and:

$$f^{(1)}(t) = \int_{-\infty}^{+\infty} h^{(1)}(\tau_1)\zeta(t-\tau_1)\mathrm{d}\tau_1 \tag{12}$$

$$f^{(2)}(t) = \int_{-\infty}^{+\infty}\int_{-\infty}^{+\infty} h^{(2)}(\tau_1,\tau_2)\zeta(t-\tau_1)\zeta(t-\tau_2)\mathrm{d}\tau_1\mathrm{d}\tau_2 \tag{13}$$

$$\vdots$$

$$f^{(m)}(t) = \int_{-\infty}^{+\infty}\cdots\int_{-\infty}^{+\infty} h^{(m)}(\tau_1,\tau_2,\ldots\tau_m)\zeta(t-\tau_1)\zeta(t-\tau_2)\ldots\zeta(t-\tau_m)\mathrm{d}\tau_1\mathrm{d}\tau_2\cdots\mathrm{d}\tau_m \tag{14}$$

here $f(t)$ is the response of the system, ζ is an input excitation, and $h^{(m)}$ is the m-th order impulse response function or also known as a Volterra kernel. The corresponding frequency-domain representation can obtained by simply taking the Fourier transform of Eqs. (11-14) (Chance et al., 1998).

$$F(\omega) = F^{(0)} + F^{(1)}(\omega) + F^{(2)}(\omega) + \cdots + F^{(m)}(\omega) \tag{15}$$

where,

$$F^{(1)}(\omega) = \frac{1}{2\pi}\int_{-\infty}^{+\infty} \delta(\omega-\omega_1)H^{(1)}(\omega-\omega_1)Z(\omega_1)d\omega_1 \tag{16}$$

$$F^{(2)}(\omega) = \frac{1}{2\pi}\int_{-\infty}^{+\infty}\int_{-\infty}^{+\infty} \delta(\omega-\omega_1-\omega_2)H^{(2)}(\omega_1,\omega_2)Z(\omega_1)Z(\omega_2)d\omega_1 d\omega_2 \tag{17}$$

$$\vdots$$

$$F^{(m)}(\omega) = \frac{1}{2\pi}\int_{-\infty}^{+\infty}\ldots\int_{-\infty}^{+\infty} \delta(\omega-\omega_1-\omega_2-\ldots-\omega_m)H^{(m)}(\omega_1,\ldots,\omega_m)Z(\omega_1)\ldots Z(\omega_n)d\omega_1\ldots d\omega_m \tag{18}$$

where, F and Z are the frequency domain counterparts of the response and excitation while $H^{(m)}$ is the m-th order GFRF, which corresponds to the m-dimenstional Fourier transform of the corresponding Volterra kernel,

$$H^{(m)}(\omega_1,\dots,\omega_m) = \frac{1}{2\pi}\int_{-\infty}^{+\infty}\dots\int_{-\infty}^{+\infty} h^{(m)}(\tau_1,\dots,\tau_m)e^{\left(-1i\sum_j^m \omega_j\tau_j\right)}\mathrm{d}\tau_1\mathrm{d}\tau_2\cdots\mathrm{d}\tau_m \tag{19}$$

In theory, the Volterra expansion could capture the interactions of an infinite number of simple harmonics. In this study, we are interested in the estimation of GFRF up to order two, i.e., LFT ($H^{(1)}(\omega_1)$) and QTF ($H^{(2)}(\omega_1,\omega_2)$).

3.2 Harmonic Probing

The idea behind HP is to probe the system with simple harmonic excitations for which the analytical expression for the response is known. To that purpose, Eq. (22) is equated to the Taylor-expanded version of the mean predictor from Eq. (7). To capture the second order effects the Taylor expansion of (7) is truncated after the quadratic term.

$$f_n = \mathcal{F}(\mathbf{x}_n) \approx \cancelto{0}{\mathcal{F}(\mathbf{0})} + \left.\frac{\partial\mathcal{F}}{\partial\mathbf{x}}\right|_{\mathbf{0}} {\mathbf{x}_n}^T + \frac{1}{2}\mathbf{x}_n \left.\frac{\partial^2\mathcal{F}}{\partial\mathbf{x}^2}\right|_{\mathbf{0}} {\mathbf{x}_n}^T + \dots \tag{20}$$

where $\mathcal{F}(\mathbf{0})$ is the bias term set equal to zero, $\left.\frac{\partial\mathcal{F}}{\partial\mathbf{x}}\right|_{\mathbf{0}}$ and $\left.\frac{\partial^2\mathcal{F}}{\partial\mathbf{x}^2}\right|_{\mathbf{0}}$ are the Jacobian and the Hessian of the mean predictor of (7) evaluated at $\mathbf{x}_n = \mathbf{0}$. Both Jacobian and Hessian can be conveniently evaluated using numerical differentiation like finite-difference schemes or automatic differentiation. In the authors' experience, symbolic differentiation is also a viable approach. However, its effectiveness is conditioned to the functional form of the NARX. Noteworthy, the Taylor expansion of (20) is necessary for converting the Kriging-NARX model into a multivariate polynomial suitable for harmonic probing. Specifically, the nonlinear terms are responsible for the generation of the inter-modulation frequencies (Billings, 2013).

Based on Eqs.(11 - 18), the discretized system response caused by a bi-chromatic excitation

$$\zeta_n = e^{\mathrm{i}\Omega_1 t_n} + e^{\mathrm{i}\Omega_2 t_n} \tag{21}$$

reads,

$$f_n = H^{(1)}(\Omega_1)e^{\mathrm{i}\Omega_1 t_n} + H^{(1)}(\Omega_2)e^{\mathrm{i}\Omega_2 t_n} + 2H^{(2)}(\Omega_1,\Omega_2)e^{\mathrm{i}(\Omega_1+\Omega_2)t_n}\dots \tag{22}$$

where $t_n = n\Delta t$. The equation above provides an analytical way to relate the response of the system to its transfer functions. Using (21) and (22), the input vector to the mean predictor from (7) can be given an analytical form.

$$\mathbf{x}_n = \begin{bmatrix} f_{n-1} \\ f_{n-2} \\ \vdots \\ f_{n-n_f} \\ \zeta_n \\ \zeta_{n-1} \\ \vdots \\ \zeta_{n-n_\zeta} \end{bmatrix}^T = \begin{bmatrix} [H^{(1)}(\Omega_1)e^{\mathrm{i}\Omega_1} + H^{(1)}(\Omega_2)e^{\mathrm{i}\Omega_2} + 2H^{(2)}(\Omega_1,\Omega_2)e^{\mathrm{i}(\Omega_1+\Omega_2)} + \ldots]e^{t_n-\Delta t} \\ [H^{(1)}(\Omega_1)e^{\mathrm{i}\Omega_1} + H^{(1)}(\Omega_2)e^{\mathrm{i}\Omega_2} + 2H^{(2)}(\Omega_1,\Omega_2)e^{\mathrm{i}(\Omega_1+\Omega_2)} + \ldots]e^{t_n-2\Delta t} \\ \vdots \\ [H^{(1)}(\Omega_1)e^{\mathrm{i}\Omega_1} + H^{(1)}(\Omega_2)e^{\mathrm{i}\Omega_2} + 2H^{(2)}(\Omega_1,\Omega_2)e^{\mathrm{i}(\Omega_1+\Omega_2)} + \ldots]e^{t_n-n_f\Delta t} \\ e^{\mathrm{i}\Omega_1 t_n} + e^{\mathrm{i}\Omega_2 t_n} \\ e^{\mathrm{i}\Omega_1(t_n-\Delta t)} + e^{\mathrm{i}\Omega_2(t_n-\Delta t)} \\ \vdots \\ e^{\mathrm{i}\Omega_1(t_n-n_\zeta\Delta t)} + e^{\mathrm{i}\Omega_2(t_n-n_\zeta\Delta t)} \end{bmatrix}^T \tag{23}$$

Note that the substituted values in the vector above are time-shifted to account for the lags in the input data.

Accordingly, the only remaining unknowns are the transfer functions which can be isolated and solved for. The classical procedure for solving for the transfer functions is completed in cascade starting from the lowest order and moving forward. When a bias term is not present, the computation begins with the linear transfer function. A harmonic balance is constructed for the terms oscillating at frequency Ω_1. This involves identifying all terms followed by $e^{i\Omega_1 t_n}$ and equating their coefficients which leads to the expression of the LTF, $H^{(1)}(\Omega_1)$. In the same manner, a harmonic balance is solved for the frequency $\Omega_1 + \Omega_2$ leading to the expression of the QTF, $H^{(2)}(\Omega_1, \Omega_2)$. However, constructing the harmonic balances is not a trivial problem from a computational point of view. Depending on the number of lags (i.e. nf and $n\zeta$), expanding Eq. (20) could result in a very lengthy expression. Employing a symbolic tool for scanning and identifying the balancing terms becomes intractable for complex models with a long memory and many lagged inputs. For that reason, a numerical harmonic probing approach is sought after.

To circumvent the need for symbolic computation, the harmonic balances are instead solved in the frequency domain numerically. The procedure is completed in cascade starting from the linear case,

$$\zeta_n = e^{i\Omega_1 t_n} \ , \ f_n^{(1)} = \hat{H}^{(1)}(\Omega_1)e^{i\Omega_1 t_n} \tag{24}$$

where ζ_n and $f_n^{(1)}$ are the monochromatic excitation and response based on a trial—inexact—value of $\hat{H}^{(1)}(\Omega_1)$ as initial guess. It follows that, if one substitute (24) into the Taylor expansion of (20) truncated up at the linear term, the harmonic balance is not verified, giving rise to a residual,

$$r_n(\hat{H}^{(1)}(\Omega_1)) = f_n^{(1)} - \left.\frac{\partial \mathcal{F}}{\partial \mathbf{x}}\right|_{\mathbf{0}} \mathbf{x}_n{}^T \tag{25}$$

where the functional dependency of $f_n^{(1)}$ and $\mathbf{x}_n^{(1)}$ on $\hat{H}^{(1)}(\Omega_1)$ is omitted for the sake of space. For the linear case, no inter-modulation of frequencies is possible, meaning that the residual will oscillate only at Ω_1.

$$\mathbf{C}^{(1)} = \{\Omega_1\}$$

where $\Omega_1 \in \Omega = [0, \ldots, \Omega_b]$. Consequently, the frequency spectrum of the residual is a Dirac delta centered at Ω_1,

$$R(\hat{H}^{(1)}(\Omega_1)) = \sum_n r_n(\hat{H}^{(1)}(\Omega_1))e^{-i\Omega_1 n\Delta t} \tag{26}$$

where $R^{(1)}(H^{(1)}(\Omega_1))$ is the frequency spectrum obtained by the Discrete Fourier Transform (DFT). Finally, the linear transfer function is obtained by minimizing the amplitude of the frequency spectrum at Ω_1,

$$H^{(1)}(\Omega_1) = \underset{\hat{H}^{(1)}(\Omega_1)}{\arg\min} |R^{(1)}(H^{(1)}(\Omega_1))| \quad \forall \Omega_1 \in \Omega \tag{27}$$

The optimization above is repeated for the entire set of frequencies Ω such that the whole frequency band of the transfer function is covered. From a practical point of view, the computation of the LTF is also possible by simpler analytical methods though they are almost always limited to first order effects. The numerical probing of the LTF presented here is for pedagogical reasons and to serve as a stepping stone towards understanding the numerical probing of the higher order terms.

The computation for the quadratic transfer function requires probing with a bichromatic excitation and a second order Volterra response,

$$\zeta_n = e^{i\Omega_1 t_n} + e^{i\Omega_2 t_n} \tag{28}$$

$$f_n^{(2)} = H^{(1)}(\Omega_1)e^{\mathrm{i}\Omega_1 t_n} + H^{(1)}(\Omega_2)e^{\mathrm{i}\Omega_2 t_n} + 2H^{(2)}(\Omega_1, \Omega_2)e^{\mathrm{i}(\Omega_1+\Omega_2)t_n} \tag{29}$$

Furthermore, the Taylor series expansion is extended to include the quadratic term.

$$f_n^{(2)} = \left.\frac{\partial \mathcal{F}}{\partial \mathbf{x}}\right|_{\mathbf{0}} \mathbf{x}_n^{(2)^T} + \frac{1}{2}\mathbf{x}_n^{(2)} \left.\frac{\partial^2 \mathcal{F}}{\partial \mathbf{x}^2}\right|_{\mathbf{0}} \mathbf{x}_n^{(2)^T} \tag{30}$$

Including the second order term is necessary for frequency inter-modulation i.e. it is the mechanism that produces the additional oscillating frequencies listed below,

$$\begin{aligned}\mathbf{C}^{(2)} = \{&\Omega_1, 2\Omega_1, 3\Omega_1, 4\Omega_1, \Omega_2, 2\Omega_2, 3\Omega_2, 4\Omega_2, \dots \\ &\Omega_1+\Omega_2, 2\Omega_1+2\Omega_2, 2\Omega_1+\Omega_2, 3\Omega_1+\Omega_2, \Omega_1+2\Omega_2, \Omega_1+3\Omega_2, \dots \\ &3\Omega_1+2\Omega_2, 2\Omega_1+3\Omega_2\}\end{aligned}$$

with $\{\Omega_1, \Omega_2\} \in \Omega \times \Omega$. As for the linear case, the system response from (29) and Taylor series expansion from (30) are recast into a residual from,

$$r_n^{(2)}(\hat{H}^{(2)}(\Omega_1, \Omega_2); \hat{H}^{(1)}(\Omega_1), \hat{H}^{(1)}(\Omega_2)) = f_n^{(2)} - \left.\frac{\partial \mathcal{F}}{\partial \mathbf{x}}\right|_{\mathbf{0}} \mathbf{x}_n^{(2)^T} - \frac{1}{2}\mathbf{x}_n^{(2)} \left.\frac{\partial^2 \mathcal{F}}{\partial \mathbf{x}^2}\right|_{\mathbf{0}} \mathbf{x}_n^{(2)^T} \tag{31}$$

with the corresponding DFT,

$$R^{(2)}(\hat{H}^{(2)}(\Omega_1, \Omega_2); \hat{H}^{(1)}(\Omega_1), \hat{H}^{(1)}(\Omega_2) = \sum_n r_n^{(2)}(\hat{H}^{(2)}(\Omega_1, \Omega_2); \hat{H}^{(1)}(\Omega_1), \hat{H}^{(1)}(\Omega_2))e^{-i\Omega_1 n\Delta t} \tag{32}$$

The optimization problem is formulated once again, now minimizing the amplitude of the sum frequency $\Omega_1 + \Omega_2$,

$$H^{(2)}(\Omega_1, \Omega_2) = \underset{\hat{H}^{(2)}(\Omega_1,\Omega_2)}{\arg\min} |R^{(2)}(\hat{H}^{(2)}(\Omega_1, \Omega_2); \hat{H}^{(1)}(\Omega_1), \hat{H}^{(1)}(\Omega_2)| \quad \forall \Omega_1, \Omega_2 \in \Omega \tag{33}$$

The idea behind the optimization is that the amplitudes of the residual can be minimized with respect to the transfer functions. Reducing the amplitude to zero implies that the coefficients for a given harmonic, $e^{i\Omega t_n}$, are in perfect balance (i.e. cancel out) which is only possible if the correct transfer function has been identified. A typical representation of the second order residual in time and frequency domain is shown below in Figure 1.

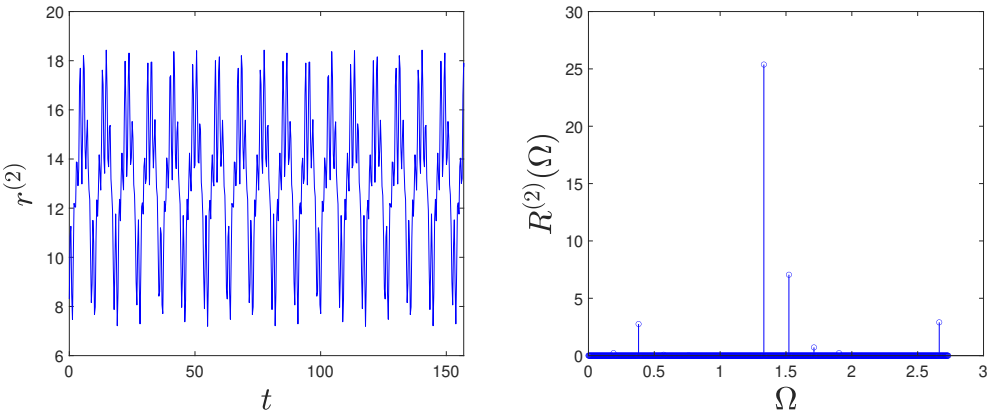

Figure 1: A typical second order residual in time and frequency domain

4. NUMERICAL CASE STUDY

The NARX and numerical harmonic probing framework were applied to a floater, limited for the time being to estimating the surge *linear* transfer function, relating the wave elevation profile ζ to the hydrodynamic surge force f on the floater. A description of the floater under study is available in Section 4.1. The validation study used synthetic time-series data whose generation is described in Section 4.2. Lastly, the obtained results are presented in Section 4.3 and 4.4.

4.1 Floater Description

The floater used for this study was the *INO WINDMOOR 12MW* floater (Souza et al., 2021), a semi-submersible structure with three columns connected by pontoons. The structure has been modelled in *Hydrostar* (Bureau Veritas., 2016) for the purposes of obtaining the transfer functions. The vessel mesh consisted of 11212 panels. Figure 2 shows a render and scale model of the floater.

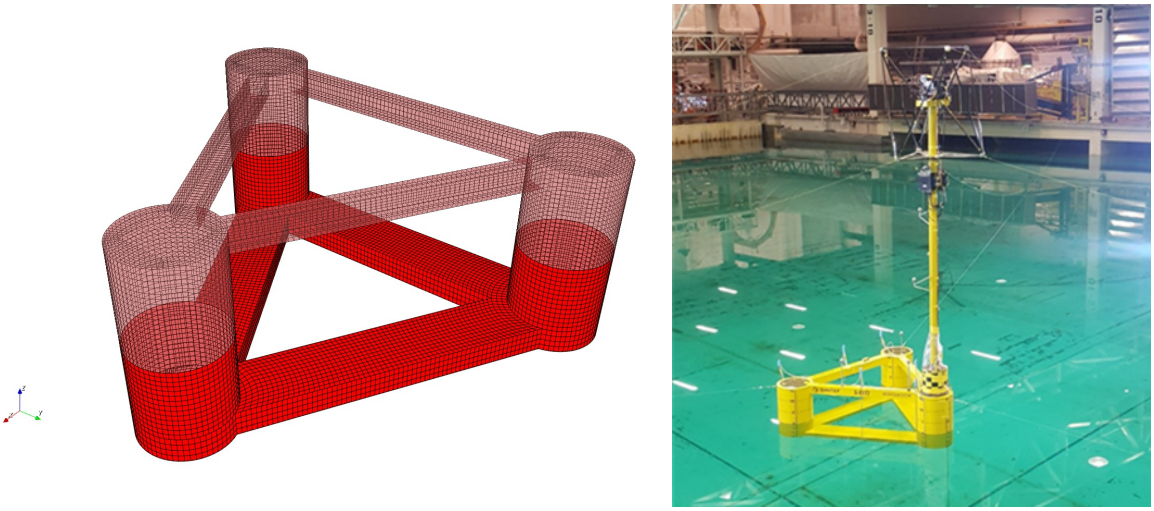

Figure 2: Panel model (Hydrostar) of the INO WINDMOOR floater (left), and a 1:40 scaled model tested at SINTEF Ocean (Thys et al., 2021) (right)

4.2 Data Generation

The synthetic data was obtained by first producing a random wave elevation profile from a JONSWAP spectrum with a significant wave height of $H_s = 0.5$ m and a period of $T_p = 13$ s. A plot of the spectrum is shown below on Figure 3.

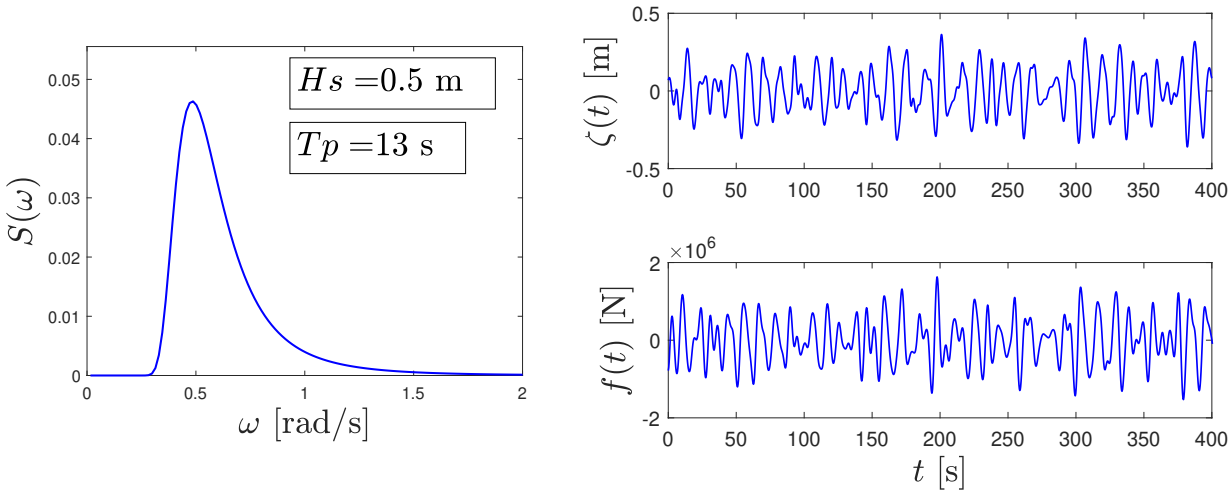

Figure 3: A JONSWAP spectrum used to generate the data (left). A wave elevation profile sample with the corresponding 1st order force exerted on the floater (right)

The transfer function of the floater computed in Hydrostar together with a wave elevation profile were used to generate a synthetic loading time-series data using the approach outlined in (Cheng et al., 2018). The Python toolbox *Snoopy* (Bureau Veritas, Research Department., 2022) was used for this purpose. The first-order force was calculated as follows:

$$f^{(1)}(t) = \mathcal{R} \sum_{m=1}^{M} |H^{(1)}(\omega_m)| \sqrt{2S(\omega_m)\Delta\omega} e^{i(\omega_m t + \epsilon_m + \phi_m)} \tag{34}$$

where $|H^{(1)}(\omega_m)|$ and ϕ_m are the amplitude and phase angle of the transfer function of the system, respectively. $S(\omega_m)$ is the JONSWAP spectrum, $\Delta\omega$ is the frequency step and ϵ_m is a random number between 0 and 2π.

4.3 NARX Setting and Results

The synthetic time-series data for the wave elevation profile, $\zeta(t)$ and force, $f(t)$ was divided into 20 segments where each segment consisted of 300 data points with a time-step, $dt = 1.2$ s. Each segment was used for training a separate Kriging-NARX model. A crucial goal of the training process is to capture the underlying physics of the actual floater. In dynamics, modeling the behaviour of a structure, depending on its complexity, could require several past states. The INO WINDMOOR floater has a relatively complex wave-body interaction that requires a longer memory. The memory effects in the Kriging-NARX model are captured in the lagged input data. This study used $n_f = 20$ and $n_\zeta = 20$ which corresponds to 24 s of lag on both the force and wave signals. The predictive capacity of each NARX was tested with a leave-one-out cross-validation technique. This process went on as follows, the 20 segments mentioned earlier were used as training data for the model producing 20 different NARX. Each one of the 20 NARX models was then validated against the remaining 19

segments. This ensured that each NARX was tested only on data that it has not seen before. The results for the 20 segments are displayed on the figure below.

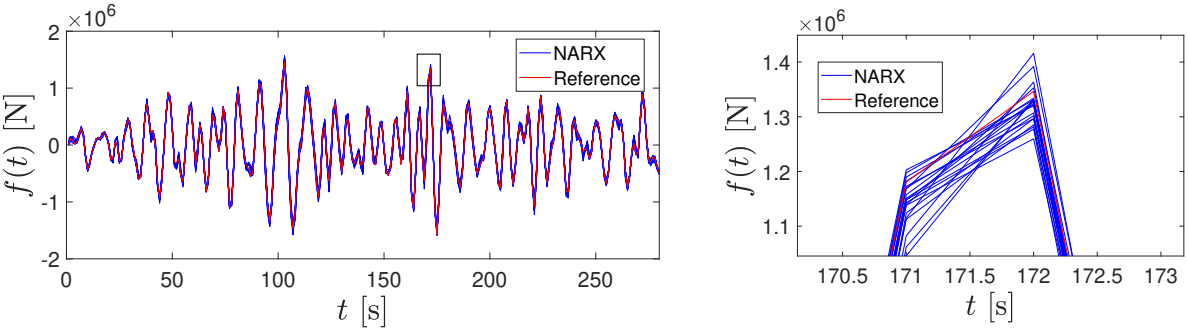

Figure 4: Comparison of the NARX predictions against the reference value (left). Magnified region from the left graphic (right)

Figure 4 shows the output of 19 NARX models (blue) validated against a different (20th) reference data-set (red). All models performed exceptionally well in estimating the force time-series. An important thing to note here is that the predictive power of the model is limited to time-series sets corresponding to a particular sea state. For a new sea state, the model needs to be retrained again.

4.4 Transfer Function Results

The numerical harmonic probing algorithm was lastly applied to the Kriging-NARX models and compared against the potential flow reference value and symbolic probing. The results for all NARX models are displayed on Figure 5.

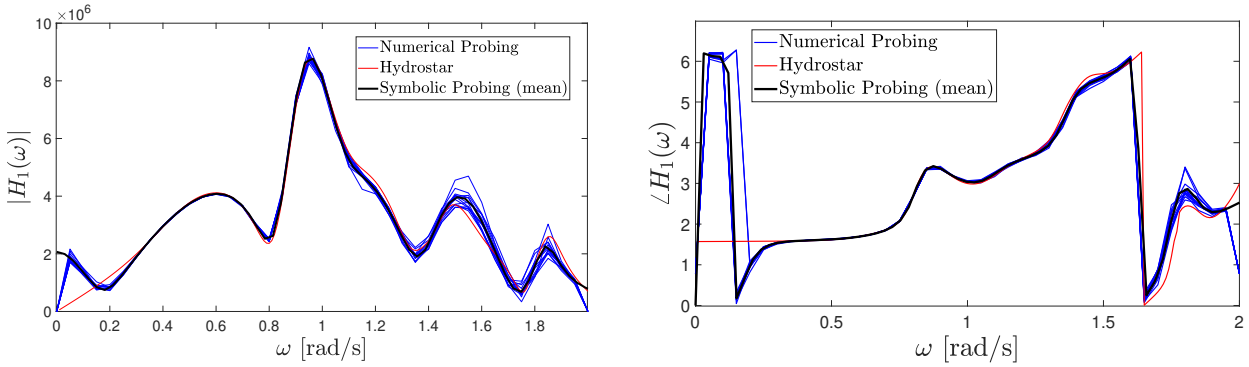

Figure 5: Amplitude (left) and phase (right) of the transfer functions obtained by numerical harmonic probing compared to the symbolic probing and the Hydrostar reference

The results from the symbolic harmonic probing, for clarity, only show the mean value. The numerical probing produced nearly identical results which serves as a proof of concept for this novel way of computing harmonic balances. Both algorithms exhibited lower uncertainty in the region between $0.3 - 1.3$ rad/s, where most of the energy from the JONSWAP (see Figure 3) was located. Inversely, the regions where less wave energy was allocated showed higher uncertainty. In terms of computational cost, the numerical probing has a relatively constant cost regardless of the order of the transfer function considered. In contrast, the cost of the symbolic probing scales nonlinearly with the order of the transfer function. For complex systems with long memory, extracting the transfer function via

symbolic calculations exceeds the computational capabilities of most computers which renders that method impractical.

5. CONCLUSION

This study investigated a new numerical approach of harmonic probing and transfer function estimation. The method was applied to a Kriging-NARX model trained on synthetic data obtained from the INO WINDMOOR 12 MW floater. The method was validated for the linear transfer function, but the generality of the approach also applies to higher order transfer functions.

The numerical probing provided nearly identical results for the linear transfer function as the classical symbolic probing. In terms of computational speed, the two methods provide comparable efficiency for extracting first order transfer functions. However, for higher order transfer functions and structures with long memory, the numerical probing is expected to exhibit a superior performance.

REFERENCES

Bayma, R. S. and Z. Q. Lang (2012). A New Method for Determining the Generalised Frequency Response Function of Nonlinear Systems. *IEEE Transactions on Circuits and Systems - I: Regular Papers, 59*, 3005–3014.

Bedrosian, E. and S. O. Rice (1971). The Output Properties of Volterra Systems (Nonlinear Systems with Memory) Driven by Harmonic and Gaussian Inputs. *Proceedings IEEE, 59*, 1688–1707.

Billings, S. A. (2013). *Nonlinear System Identification*. West Sussex, United Kingdom: John Wiley and Sons.

Bureau Veritas. (2016). Hydrostar for Experts: User Manual.

Bureau Veritas, Research Department. (2022). Snoopy Library. https://bv-dr.gitlab.io/Snoopy/.

Chance, J. E., K. Worden, and G. R. Tomlinson (1998). Frequency Domain Analysis of NARX Neural Networks. *Journal of Sound and Vibration, 213*, 915–41.

Cheng, Z., Z. Gao, and T. Moan (2018). Hydrodynamic Load Modeling and Analysis of a Floating Bridge in Homogeneous Wave Conditions. *Marine Structures, 59*, 122–141.

Faltinsen, O. M. (1990). *Sea Loads on Ships and Offshore Structures*. Cambridge, United Kingdom: Cambridge University Press.

Krige, D. G. (1951). A Statistical Approach to Some Basic Mine Valuation Problems on the Witwatersrand. *Journal of The South African Institute of Mining and Metallurgy, 52*, 119–139.

Lataniotis, C., D. Wicaksono, S. Marelli, and B. Sudret (2022). UQLab User Manual - Kriging (Gaussian Process Modeling). Technical report, Chair of Risk, Safety and Uncertainty Quantification, ETH Zurich, Switzerland. Report UQLab-V2.0-105.

Leontaritis, I. J. and S. A. Billings (1985a). Input-Output Parametric Models for Nonlinear Systems, Part I - Deterministic Nonlinear Systems. *International Journal of Control, 41*, 303–28.

Leontaritis, I. J. and S. A. Billings (1985b). Input-Output Parametric Models for Nonlinear Systems, Part II - Stochastic Nonlinear Systems. *International Journal of Control, 41*, 329–44.

Molin, B. (2023). *Offshore Structure Hydrodynamics*. Cambridge, United Kingdom: Cambridge University Press.

Peyton-Jones, J. C. and S. Billings (1989). Recursive Algorithm for Computing the Frequency Response of a Class of Non-linear Difference Equation Model. *International Journal of Control, 50*, 1925–1950.

Rasmussen, C. E. and K. I. Williams (2006). *Gaussian Processes for Machine Learning*. Cambridge, Massachusetts: MIT Press.

Santner, T. J., B. J. Williams, and W. I. Notz (2019). *The Design and Analysis of Computer Experiments* (2 ed.). 233 Spring Street, New York, NY 10013, U.S.A.: Springer.

Sauder, T. (2021). Empirical Estimation of Low-Frequency Nonlinear Hydrodynamic Loads on Moored Structures. *Applied Ocean Research, 117*, 102895.

Souza, C., P. A. Berthelsen, L. Eliassen, E. Bachynski, E. Engebretsen, and H. Haslum (2021). Definition of the INO WINDMOOR 12MW Base Case Floating Wind Turbine. Technical report, SINTEF, Trondheim, Norway.

Thys, M., C. Souza, T. Sauder, P. A. Berthelsen, E. Engebretsen, and H. Haslum (2021). Experimental Investigation of the Coupling Between Aero and Hydrodynamic Loads on a 12MW Semi-Submersible Floating Wind Turbine. *Proceedings of the ASME 2021 40th International Conference on Ocean, Offshore and Arctic Engineering OMAE2021, 9*.

Tsang, K. M. and S. A. Billings (1992). Reconstruction of Linear and Non-linear Continuous Time Models from Discrete Time Sampled-Data Systems. *Mechanical Systems and Signal Processing, 6*, 69–84.

Weiner, N. (1942). Response of a Nonlinear Device to Noise. Radiation Lab, MIT, Cambride, MA.

Worden, K., W. E. Becker, T. J. Rogers, and E. J. Cross (2018). On the Confidence Bounds of Gaussian Process NARX Models and Their Higher-Order Frequency Response Functions. *Mechanical Systems and Signal Processing 104*, 118–223.

Worden, K., G. Manson, and E. J. Cross (2012). Higher-Order Frequency Response Functions from Gaussian Process NARX Models. *Proceedings of ISMA2012-USD2012, 1*, 2575–90.

Worden, K. and G. R. Tomlison (2001). *Nonlinearity in Structural Dynamics: Detection, Identification and Modelling*. Dirac House, Temple Back, Bristol BS1 6BE, UK: Institute of Physics Publishing.